

# Laboratory constraints on chameleon dark energy and power-law fields

J. H. Steffen<sup>1</sup>, A. Upadhye<sup>2</sup>, A. Baumbaugh<sup>1</sup>, A. S. Chou<sup>1</sup>, P. O. Mazur<sup>1</sup>, R. Tomlin<sup>1</sup>, A. Weltman<sup>3</sup>, and W. Wester<sup>1</sup>

<sup>1</sup>*Fermi National Accelerator Laboratory, PO Box 500, Batavia, IL 60510*

<sup>2</sup>*Kavli Institute for Cosmological Physics, University of Chicago, IL 60637*

<sup>3</sup>*Astrophysics, Cosmology and Gravity Centre, University of Cape Town, Rondebosch, Private Bag, 7700, South Africa*

(Dated: October 22, 2018)

We report results from the GammeV Chameleon Afterglow Search—a search for chameleon particles created via photon/chameleon oscillations within a magnetic field. This experiment is sensitive to a wide class of chameleon power-law models and dark energy models not previously explored. These results exclude five orders of magnitude in the coupling of chameleons to photons covering a range of four orders of magnitude in chameleon effective mass and, for individual chameleon models, exclude between 4 and 12 orders of magnitude in chameleon couplings to matter.

PACS numbers: 95.36.+x, 95.35.+d, 14.80.Va, 98.80.-k

**Introduction:** A wealth of observational evidence indicates that the universe is undergoing a phase of accelerated expansion, for which a promising class of explanations is scalar field “dark energy” with negative pressure [1]. Such a field is expected to couple to Standard Model particles with gravitational strength and would mediate a new “fifth” force, but fifth forces are excluded by experiments from solar system to submillimeter scales. Three known ways to hide dark energy-mediated fifth forces include: weak or pseudoscalar couplings between dark energy and matter [2]; effectively weak couplings locally [3]; and an effectively large field mass locally, as in chameleon theories [4–6].

Chameleons are scalar (or pseudoscalar) fields with a nonlinear potential and a coupling to the local energy density. They evade fifth force constraints by increasing their effective mass in high-density regions of the universe, while remaining light on cosmological scales. Gravity experiments in the lab [7] and in space [4, 5] can exclude chameleons with gravitational strength matter couplings, but strongly coupled chameleons evade these constraints [8, 9]. Casimir force experiments rule out strongly coupled chameleons [10], but are ineffective for a large class of potentials commonly used to model dark energy. Collider data exclude extremely strongly coupled chameleons [11]. In this Letter, we place new constraints on chameleon couplings with a search focused on photon/chameleon interactions.

Photon-coupled chameleons may be detected through laser experiments [12] or excitations in radio frequency cavities [13]. In laser experiments, photons travelling through a vacuum chamber immersed in a magnetic field oscillate into chameleons. They are then trapped through the chameleon mechanism by the dense walls and windows of the chamber since their higher effective mass within those materials creates an impenetrably large potential barrier [12, 14, 15]. After a population of chameleons is produced, the laser is turned off and a photodetector exposed in order to observe the photon afterglow as trapped chameleons oscillate

back to photons. The original GammeV experiment included a search for this afterglow and set limits on photon/chameleon couplings below collider constraints for a limited set of dark energy models [12]. The experiment presented here, the GammeV Chameleon Afterglow Search (CHASE), bridges the gap between GammeV and collider constraints, improves sensitivity to both matter and photon couplings to chameleons, and probes a broad class of chameleon models.

**Chameleon Models:** We consider actions of the form

$$S = \int d^4x \sqrt{-g} \left( \frac{1}{2} M_{\text{Pl}}^2 R - \frac{1}{2} \partial_\mu \phi \partial^\mu \phi - V(\phi) - \frac{1}{4} e^{\beta_\gamma \phi / M_{\text{Pl}}} F^{\mu\nu} F_{\mu\nu} + \mathcal{L}_m(e^{2\beta_m \phi / M_{\text{Pl}}} g_{\mu\nu}, \psi_m^i) \right) \quad (1)$$

where the reduced Planck mass  $M_{\text{Pl}} = 2.43 \times 10^{18}$  GeV,  $\mathcal{L}_m$  the Lagrangian for matter fields  $\psi_m^i$ , and  $\beta_\gamma$  and  $\beta_m$  are dimensionless chameleon couplings to photons and matter respectively (often expressed as  $g_\gamma = \beta_\gamma / M_{\text{Pl}}$  and  $g_m = \beta_m / M_{\text{Pl}}$ ). We assume universal matter couplings.

The dynamics of the scalar field are governed by an effective potential that depends on a scalar field potential  $V(\phi)$ , the background density  $\rho_m$  of nonrelativistic matter, and the electromagnetic field Lagrangian density  $\rho_\gamma = F^{\mu\nu} F_{\mu\nu} / 4 = (B^2 - E^2) / 2$  (for pseudoscalars  $\rho_\gamma = F^{\mu\nu} \tilde{F}_{\mu\nu} / 4 = \vec{B} \cdot \vec{E}$ ):

$$V_{\text{eff}}(\phi, \vec{x}) = V(\phi) + e^{\frac{\beta_m \phi}{M_{\text{Pl}}}} \rho_m(\vec{x}) + e^{\frac{\beta_\gamma \phi}{M_{\text{Pl}}}} \rho_\gamma(\vec{x}). \quad (2)$$

A simple, well-studied class of chameleon models has a potential of the form [6]

$$V(\phi) = M_\Lambda^4 e^{\kappa \left( \frac{\phi}{M_\Lambda} \right)^N} \approx M_\Lambda^4 \left[ 1 + \kappa \left( \frac{\phi}{M_\Lambda} \right)^N \right]. \quad (3)$$

where  $N$  is a real number and  $M_\Lambda = \rho_{\text{de}}^{1/4} \approx 2.4 \times 10^{-3}$  eV is the mass scale of the dark energy density  $\rho_{\text{de}}$  and  $\kappa$  is a dimensionless constant. While the constant term in this potential causes cosmic acceleration that is indistinguishable from a cosmological constant when using standard

techniques of cosmological surveys, the local dynamics from the power-law term can be probed in laboratory experiments.

Following the derivations in [16, 17] the conversion probability between photons and chameleons is

$$\mathcal{P}_{\gamma \leftrightarrow \phi} = \left( \frac{2\omega\beta_\gamma B}{M_{\text{Pl}} m_{\text{eff}}^2} \right)^2 \sin^2 \left( \frac{m_{\text{eff}}^2 \ell}{4\omega} \right) \hat{k} \times (\hat{x} \times \hat{k}). \quad (4)$$

Here,  $\omega$  is the particle energy,  $m_{\text{eff}} = \sqrt{V_{\text{eff},\phi\phi}}$  is the effective chameleon mass in the background fields,  $\ell$  is the distance travelled through the magnetic field, and  $\hat{k}$  is the particle direction.

When a superposed photon/chameleon wavefunction strikes an opaque surface of the vacuum chamber, there is a model-dependent phase shift  $\xi_{\text{ref}}$  between the two components and a reduction in photon amplitude due to absorption. A glass window, however, performs a quantum measurement—photons are transmitted while chameleons reflect. Surface roughness and small misalignments of the windows cause the velocities of trapped chameleons to become isotropic. The decay rate of a chameleon to a photon  $\Gamma_{\text{dec},\gamma}$ , is found by averaging over initial directions and positions. The observable afterglow rate per chameleon  $\Gamma_{\text{aft}}$  is found by averaging over only trajectories that allow a photon to reach the detector. Once the experimental geometry is specified, these rates can be computed numerically [17].

A single parameter  $\eta$  is useful to describe the chameleon effect and to determine whether a particle will be trapped inside the chamber. If the chameleon mass in the chamber is dominated by the matter coupling, then  $m_{\text{eff}} \propto \rho_{\text{m}}^\eta$  where  $\eta = (N - 2)/(2N - 2)$  [17]. The largest value of  $\eta$  with integer  $N$  is  $\eta = 3/4$  for  $N = -1$ ;  $\phi^4$  theory ( $N = 4$ ), has  $\eta = 1/3$ . Here, we do not consider  $0 < N < 2$  since their potentials are either unbounded from below or do not exhibit the chameleon effect.

**Apparatus:** The design of the CHASE apparatus is shown in Fig. 1. In addition to the windows at the ends of the vacuum chamber, we centered two 2.5 cm diameter BK7 glass windows in the 6.3 cm diameter cold bore of a Tevatron dipole magnet. These windows divide the magnetic field into three partitions of lengths 1.0 m, 0.3 m, and 4.7 m. The shorter partition lengths provide sensitivity to larger-mass chameleons and were chosen to minimize the number of regions of mass insensitivity that occur when the partition lengths are simultaneous multiples of the photon/chameleon oscillation length (see Eq. 4).

For a fixed magnetic field there are limits to the smallest and largest detectable  $\beta_\gamma$ —small  $\beta_\gamma$  produce small afterglow signals while with large  $\beta_\gamma$  the chameleon population will decay before the detector can be exposed. For CHASE, we implement an automated transition between filling the cavity and observing an afterglow. This requires turning off the laser, closing the laser-side gate valve, removing the mirror that deflects the laser into

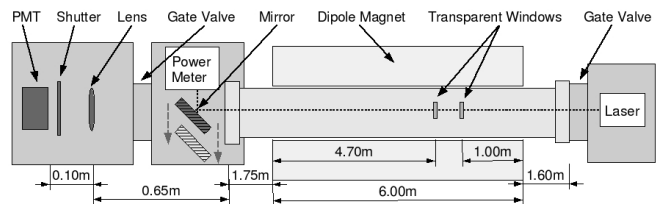


FIG. 1: Schematic of the CHASE apparatus.

the power meter, and opening the PMT-side gate valve. Our sensitivity to large  $\beta_\gamma$  is further improved by operating at a variety of lower magnetic fields, which lengthen the decay time of the chameleon population and provide overlapping regions of sensitivity. A mechanical shutter (chopper) modulates any afterglow signal allowing real-time measurement of the PMT dark rate and improving sensitivity to low afterglow rates (small  $\beta_\gamma$ ).

To maximize our sensitivity to different chameleon models, the CHASE vacuum system uses ion pumps and cryogenic pumping on the cold ( $\sim 4$  K) bore of the magnet. This design leaves no port through which chameleons can be exhausted to the room and allows CHASE to probe  $\eta$  as low as 0.1. This sensitivity is primarily due: 1) to the large matter density ratio  $\rho_{\text{m}}(\text{wall})/\rho_{\text{m}}(\text{chamber}) \sim 10^{14}$  between the walls of the vacuum chamber and its interior and 2) the large masses probed by the shortest partition of the magnetic field.

**Data:** We collected data in 14 configurations—seven vertically-oriented, dipole magnetic field values (0.050, 0.090, 0.20, 0.45, 1.0, 2.2, and 5.0 Telsa) and both vertical and horizontal polarizations of the electric field of the laser photons. The magnetic field was determined from field vs. current calibrations that are precise to better than 1%. We repeated measurements at 5.0T for a total of 16 science “runs”.

A 5.1cm diameter lens focuses the photons coming from the apparatus onto the photocathode of our Hamamatsu H7422P-40 PMT. The factory measured quantum efficiency of the PMT is 0.45 with a typical collection efficiency of 0.70. The threshold on the PMT discriminator is set to record 97% of the single photoelectrons while rejecting noise. We estimate our optical transport efficiency through the lens, the PMT-side vacuum window, and the windows in the magnet bore to be 0.96 by assigning an equal loss of 0.99 (based upon factory specifications) to each of the four elements. Thus, our photon detection efficiency is  $\epsilon_{\text{det}} = 0.29$ . Since a chameleon afterglow signal requires two factors of Eq. (4)—one to produce a chameleon and another to regenerate a photon—our sensitivity to  $\beta_\gamma$  scales only as the fourth root of  $\epsilon_{\text{det}}$ , and a modest uncertainty (estimated to be smaller than 20%) has only a  $< 5\%$  effect on  $\beta_\gamma$ .

A single science run consists of shining a frequency-doubled Continuum Surelite I-20 Nd:YAG laser with 20 Hz of 5 ns pulses through the cavity for ten minutes,

then exposing the PMT to the apparatus for 14 minutes while cycling the shutter open and closed in  $\sim 15$  second intervals each. At the highest magnetic field the filling and observation stages are extended to 5 hours and 45 minutes respectively to improve our sensitivity to low  $\beta_\gamma$ . The average input laser power is 3.5 Watts with  $\pm 0.1$  Watt fluctuations (which also have negligible effect on our sensitivity). Before and after each science run, there is a 15 minute calibration run which we use to measure three quantities: the excess photon rate coming from the apparatus (due in part to discharge from the ion pumps), random fluctuations of that excess, and its run-to-run variation. Our data acquisition system saturates at approximately 300 Hz while the typical counting rate with the shutter-closed is  $\sim 28$  Hz. We see an excess rate of  $1.15 \pm 0.08$  Hz with the shutter open. The shutter-open data has 0.94 Hz of variation beyond Poisson fluctuations of 1.34 Hz. At most 0.40 Hz of this variation could be attributed to run-to-run changes in the mean offset.

Vacuum pressure measurements are taken before and after the observation stage using two ion gauges (one at either end of the magnet). We turn these gauges off during observation since, when on, we observe hundreds of photons per second from them. Frequent measurements of the residual gases show 87%  $\text{H}_2$ , 4%  $\text{H}_2\text{O}$ , and  $\text{N}_2$  and  $\text{CO}$  (28 amu) combine for 9%. Using the factory calibration of the gauges for the various gas species, we find that our vacuum pressure was always better than  $1.6 \times 10^{-9}$  torr at 3.5K (a density of  $3.2 \times 10^{-14}$  g/cm<sup>3</sup> compared with  $\sim 2.5$  g/cm<sup>3</sup> for the glass windows).

Following the operation of the laser, we observe a decaying rate of photons dubbed “orange glow”. While its cause is unknown, its properties distinguish it from a scalar or pseudoscalar chameleon signal. First, the orange glow is isolated to the red and orange parts, rather than the expected 532nm green, of the electromagnetic spectrum (found using a series of 40nm-wide filters placed in front of the PMT). Second, it is independent of both the strength of the magnetic field and the laser polarization. Finally, the amplitude of the orange glow depends upon the temperature of the magnet bore. Virtually disappearing at room temperature, it increases until reaching several hundred Hz in amplitude at temperatures near 4 K.

A series of independent “orange glow runs” similar to the nominal science run show that the temporal shape of the orange glow is reproducible and, following a steep drop of a few tens of seconds, is well fit by an exponential with an initial amplitude and decay time of  $6.9 \pm 2.9$  Hz and  $130 \pm 40$  sec respectively.[21] We eliminate the fast decaying components of the orange glow by ignoring the initial  $\sim 120$  seconds of data from each science run. This cut limits our sensitivity to large photon couplings in each run to  $\beta_\gamma \lesssim (6 \times 10^{13})(5\text{T}/B)$  (data at lower magnetic fields compensates for this limitation).

**Analysis:** For the CHASE geometry, the rates  $\Gamma_{\text{dec},\gamma}$

and  $\Gamma_{\text{aft}}$  are computed in [17]. We extend those calculations to greater  $m_{\text{eff}}$  using a Monte Carlo simulation. We account for the absorption of photon amplitude and the differences in the induced phase shift  $\xi_{\text{ref}}$  between the  $s$  and  $p$  polarizations at each reflection from the stainless steel surfaces. We measured the amplitude reflectivity of the magnet bore material (averaged over all incident angles) to be  $0.53 \pm 0.04$  by placing samples into an integrating sphere illuminated with 532nm laser light. Given these rates, the population  $N_\phi$  of chameleons in the vacuum chamber is found by integrating

$$\frac{dN_\phi}{dt} = F_\gamma(t)\mathcal{P}_{\gamma \leftrightarrow \phi} - N_\phi(t)\Gamma_{\text{dec},\gamma} \quad (5)$$

where  $F_\gamma(t)$  is the rate that laser photons stream through the chamber. Afterglow photons emerge and hit the PMT at a rate  $F_{\text{aft}}(t) = \epsilon_{\text{det}}N_\phi(t)\Gamma_{\text{aft}}$ .

For a given  $\vec{B}$ , each chameleon model—specified by its mass  $m_{\text{eff}}$  in the vacuum chamber, its photon coupling  $\beta_\gamma$ , and the chameleon potential  $V(\phi)$ —has a characteristic afterglow signal. We compute this signal as a function of the magnetic field and the chameleon model parameters. From the raw data binned to the  $\sim 15$  sec shutter cycle (e.g., Fig. 2) we subtract the 1.15 Hz excess rate from the ion pumps and the mean dark rate measured with the shutter-closed data for that run. Statistical fluctuations including the observed excess are included in the uncertainty of each datum. Data for all science runs with a given laser polarization and all orange glow runs (which have  $\vec{B} = 0$ ) are simultaneously analyzed using the Profile Likelihood method [18]. As nuisance parameters we include a common, exponentially decaying signal, which eliminates the long-decay tail of the orange glow, and each run is allowed an independent constant offset constrained by the possible 0.40 Hz run-to-run variations in the ion pump glow. We compare the  $\chi^2$  for the chameleon model with that for the model where no chameleon is present. Any chameleon model whose  $\chi^2$  is greater by 6.0 is excluded to 95% confidence.

**Results:** Analysis of our data shows no evidence for a photon-coupled chameleon. Figure 3 shows all of the residuals in the science data for the no chameleon model. The mean and RMS of these residuals are 0.05 and 1.35 Hz for pseudoscalar couplings ( $\chi^2 = 421$  with 471 degrees of freedom (DOF)) and 0.06 and 1.62 Hz for scalar couplings ( $\chi^2 = 502$  with 472 DOF). Fig. 4 shows parameters excluded to 95% confidence for scalars and pseudoscalars assuming  $m_{\text{eff}}$  dependence on  $B$  to be negligible and  $\xi_{\text{ref}} = 0$ . These constraints reach four significant milestones. First, they bridge the nearly three order of magnitude gap between bounds on  $\beta_\gamma$  from GammeV and from colliders [11]. Second, they exclude a range of  $\beta_\gamma$  spanning four orders of magnitude at masses around the dark energy scale ( $2.4 \times 10^{-3}$  eV). Third, they rule out photon couplings roughly an order of magnitude below previous limits in this mass range where

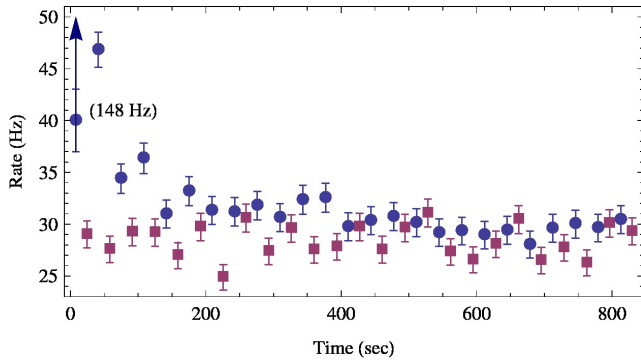


FIG. 2: Example of CHASE raw data given as the observed PMT rate vs. time. Blue circles and red squares are data with the shutter open and closed respectively. The left most datum would appear off the scale at 148Hz.

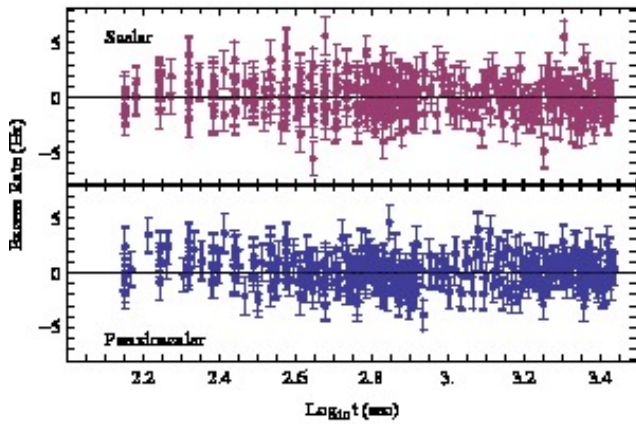


FIG. 3: Residuals from the null model for all CHASE science data. The lower panel is for pseudoscalar and the upper for scalar chameleons. Data for all magnetic fields are overlaid.

$\beta_\gamma < 7.1 \times 10^{10}$  for scalar and  $\beta_\gamma < 7.6 \times 10^{10}$  for pseudoscalar chameleons. Finally, they are sensitive to chameleon dark energy models and chameleon power-law models where  $\eta > 0.1$ , including  $V \propto \phi^4$ .

Figure 5 shows CHASE constraints (at 95%) for select potentials given by Eq. (3). These limits truncate at low  $\beta_m$  by the requirement that chameleons reflect from the chamber walls, at high  $\beta_m$  by destructive interference at large  $m_{\text{eff}}$  (see Fig. 4), and at low  $\beta_\gamma$  by undetectably small signals. Not surprisingly, theories with the largest  $\eta$  are excluded over the greatest range of  $\beta_m$ . These constraints complement those from torsion pendula, which probe  $\beta_m \sim 1$ , and are consistent with constraints from Casimir force measurements for  $N = 4$  [10]. CHASE data exclude chameleons spanning five orders of magnitude in photon coupling and over 12 orders of magnitude in matter coupling for individual models. They probe a wide range of chameleon models, and give significantly improved constraints for cosmologically interesting

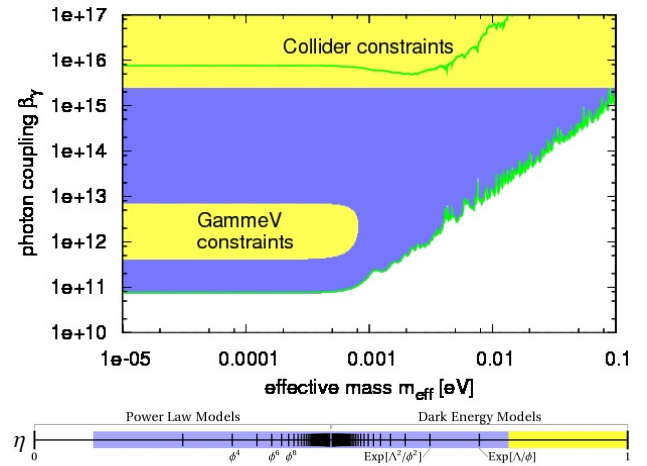


FIG. 4: Top: Scalar (solid) and pseudoscalar (outline) constraints, at 95% confidence, in the  $(m_{\text{eff}}, \beta_\gamma)$  plane for  $\xi_{\text{ref}} = 0$ . Bottom: Chameleon models probed by CHASE as parameterized by  $\eta$ . GammeV sensitivity is yellow while CHASE sensitivity is blue.

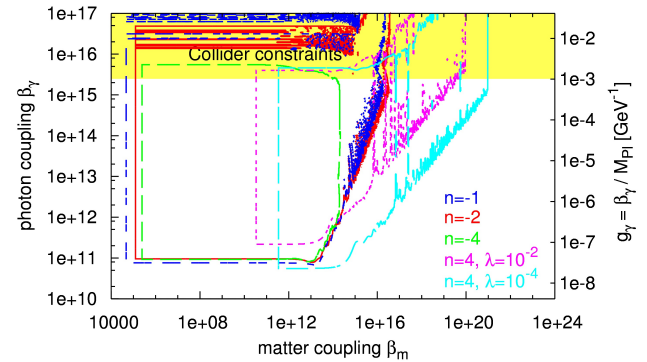


FIG. 5: 95% confidence-level constraints on chameleons with power law potentials (3). For potentials with  $N < 0$  we set  $\kappa = 1$ ; for  $\phi^4$  theory ( $N = 4$ ), we use the standard  $\kappa = \lambda/4!$ .

chameleon dark energy models.

*Acknowledgements:* We thank the staff of the Fermilab Technical Division Test and Instrumentation Department, the Fermilab Particle Physics Division mechanical design and electrical engineering groups, and the vacuum experts of the Fermilab Accelerator Division. This work is supported by the U.S. Department of Energy under contract No. DE-AC02-07CH11359 as well as by the Kavli Institute for Cosmological Physics under NSF contract PHY-0114422.

- 
- [1] R. R. Caldwell, R. Dave, and P. J. Steinhardt. *Phys. Rev. Lett.*, 80:1582, 1998.
  - [2] J. A. Frieman, C. T. Hill, A. Stebbins, and I. Waga. *Phys.*

- Rev. Lett.*, 75:2077–2080, 1995.
- [3] G. R. Dvali, G. Gabadadze, and M. Porrati. *Phys. Lett. B*, 485:208–214, 2000.
- [4] J. Khoury and A. Weltman. *Phys. Rev. Lett.*, 93, 2004. 171104.
- [5] J. Khoury and A. Weltman. *Phys. Rev. D*, 69, 2004. 044026.
- [6] Ph. Brax, C. van de Bruck, A.-C. Davis, J. Khoury, and A. Weltman. *Phys. Rev. D*, 70, 2004. 123518.
- [7] E. G. Adelberger et al. *Prog. Part. Nucl. Phys.*, 62:102–134, 2009.
- [8] D. F. Mota and D. J. Shaw. *Phys. Rev. Lett.*, 97, 2006. 151102.
- [9] D. F. Mota and D. J. Shaw. *Phys. Rev. D.*, 75, 2007. 063501.
- [10] P. Brax, C. van de Bruck, A. C. Davis, D. F. Mota, and D. J. Shaw. *Phys. Rev. D*, 76:124034, 2007. ePrint arXiv:0709.2075.
- [11] P. Brax, C. Burrage, A.-C. Davis, D. Seery, and A. Weltman. *JHEP*, 0909:128, 2009. e-print arXiv:0904.3002.
- [12] A. S. Chou et al. *Phys. Rev. Lett*, 102, 2009. 030402.
- [13] G. Rybka et al. *Phys. Rev. Lett.*, 105(5):051801, 2010.
- [14] M. Ahlers et al. *Phys. Rev. D.*, 77:015018, 2008.
- [15] H. Gies, D. F. Mota, and D. J. Shaw. *Phys. Rev. D*, 77:025016, 2008.
- [16] G. Raffelt and L. Stodolsky. *Phys. Rev. D*, 37:1237–1249, 1988.
- [17] A. Upadhye, J. H. Steffen, and A. Weltman. *Phys. Rev. D*, 81:015013, 2010.
- [18] W. A. Rolke, A. M. Lopez, and J. Conrad. *NIM A*, 551:493, 2005.
- [19] A.E. Nelson and J. Walsh. *Phys. Rev. D*, 77(9):095006, 2008.
- [20] P. Brax and C. Burrage. 2010. arXiv:1009.1065.
- [21] While we suspect that the orange glow is of conventional origin, such as impurities in the glass windows or on the vacuum chamber surfaces, exotic physics such as kinetic mixing with a spin-1 chameleon [19] or chameleon induced atomic transitions [20] have not been excluded.